Journal of Power Sources 195 (2010) 3830–3840

Contents lists available at ScienceDirect

Journal of Power Sources

journal homepage: www.elsevier.com/locate/jpowsour

Measurement of relative permeability of fuel cell diffusion media

I.S. Hussaini, C.Y. Wang*

Department of Mechanical and Nuclear Engineering, and Electrochemical Engine Center (ECEC), The Pennsylvania State University, University Park, PA 16802, USA

ARTICLE INFO

Article history:
Received 6 November 2009
Received in revised form
20 December 2009
Accepted 22 December 2009
Available online 14 January 2010

Keywords:
Relative permeability
Diffusion media
PEM fuel cell
Experimental

ABSTRACT

Gas diffusion layer (GDL) in PEM fuel cells plays a pivotal role in water management. Modeling of liquid water transport through the GDL relies on knowledge of relative permeability functions in the in-plane and through-plane directions. In the present work, air and water relative permeabilities are experimentally determined as functions of saturation for typical GDL materials such as Toray-060, -090, -120 carbon paper and E-Tek carbon cloth materials in their plain, untreated forms. Saturation is measured using an ex situ gravimetric method. Absolute and relative permeability functions in the two directions of interest are presented and new correlations for in-plane relative permeability of water and air are established.

1. Introduction

Gas diffusion layer in polymer electrolyte membrane (PEM) fuel cells is a porous layer placed between the catalyst layer and gas channel. It performs three important functions: providing pathways for reactants from gas channel to catalyst layer, conducting heat and electrons from catalyst layer to the bi-polar plate and transporting product liquid water away from the catalyst layer surface and into the gas channels [1]. Transport of liquid water through a GDL at fuel cell operating conditions occurs by capillary action and numerous studies have been documented in fuel cell literature modeling this mechanism [2], following a two-phase theory first proposed by Wang et al. [3].

Transport of fluids in porous media is described using Darcy's law which is an empirical constitutive relation for creeping flow [4]. For a multi-phase system, it is given by

$$u_i = -\frac{kk_{r,i}}{\mu_i}\nabla p_i \tag{1}$$

where u_i is the superficial velocity of phase i given by Q_i/A. For the air–water system in a fuel cell, Eq. (1) can be combined using capillary pressure ($p_c = p_a - p_w$) to give water velocity as

$$u_w = \frac{kk_{rw}}{\mu_w}\left[\frac{dp_c}{dx} - \frac{dp_a}{dx}\right] \tag{2}$$

Water relative permeability and capillary pressure are the two most important properties of the porous medium which control liquid water transport. They represent macroscopic manifestation of fluid–fluid interaction at a microscopic level in the porous matrix and are generally expressed as functions of water saturation. Comparatively, relative permeability is a far more important parameter than capillary pressure because it is un-bounded and can vary over several orders of magnitude over the range of saturations encountered in a fuel cell. Capillary pressure, however, does not show as much a variation and conforms to the pore structure according to Young–Laplace equation. A comprehensive overview of literature efforts to measure capillary pressure in GDL media is given by Gostick et al. [5].

However, measurement of relative permeability of GDL has received little attention. Some early attempts to measure air relative permeability were reported in [6,7]. Not much information is available in literature on the direct experimental measurement of water relative permeability except for the recent work reported by Sole [8]. Alternative numerical approaches using pore network models to simulate capillary motion of liquid through the pores and throats have also been applied by several researchers without experimental validation [9–11].

In the present study, experimental measurement of absolute and relative permeabilities in the through- and in-plane directions for typical GDL materials such as Toray TGP-H-060, -090 and -120 carbon paper and E-Tek carbon cloth materials in their plain, untreated forms are presented. Measurements are carried out at flow rates such that the pore Reynolds number and capillary number are in the same regime as those encountered in actual fuel cell operation.

* Corresponding author. Tel.: +1 814 863 4762; fax: +1 814 863 4848.
E-mail address: cxw31@psu.edu (C.Y. Wang).

0378-7753/$ – see front matter © 2010 Elsevier B.V. All rights reserved.
doi:10.1016/j.jpowsour.2009.12.105

Nomenclature

A	cross-sectional area (m^2)
c	compression
Ca	capillary number
k	absolute permeability (m^2)
k_r	relative permeability
m	mass (kg)
p	pressure (Pa)
Q	flow rate ($m^3\,s^{-1}$)
t	thickness (m)
u	superficial velocity ($m\,s^{-1}$)
V	volume (m^3)
ε	porosity
μ	viscosity ($N\,s\,m^{-2}$)
ρ	density ($kg\,m^{-3}$)
σ	surface tension ($N\,m^{-1}$)

Subscripts

0	uncompressed state
a	air
c	compressed state
def	defending fluid
inv	invading fluid
l	liquid
w	water

2. Experimental

A brief overview of the techniques for measuring relative permeability is given here, followed by a description of the design of experimental apparatus for through- and in-plane flows. Details of the procedure adopted for measuring parameters such as absolute permeability, porosity, saturation and relative permeability are also described.

2.1. Measurement techniques

Relative permeability of a porous sample to a fluid phase is measured either by steady-state or unsteady-state methods [12].

1. Unsteady-state methods: In these methods, the core is pre-saturated with one fluid which is then displaced by injecting the other fluid. Flow rates of the two phases are measured at the outlet in order to determine the velocity of saturation front within the core using Buckley–Leverett theory [13,14]. These methods are therefore applicable under conditions that satisfy the Buckley–Leverett model, namely, presence of a stable displacement front, high pressure gradients and negligible capillary effects.
2. Steady-state methods: In these methods, the fluids are passed at a known ratio until saturation and pressure reach a steady state. Relative permeabilities are then obtained by direct application of Darcy's law (Eq. (1)). Steps are taken to minimize the gradient in saturation so that a uniform capillary pressure is maintained. By varying the ratio of the fluids, progressive increase in saturation is achieved. A drawback of these methods is that they require several test runs in order to achieve the full spectrum of saturations.

GDL materials are generally 200–400 μm thick which renders them unsuitable for relative permeability measurement by unsteady-state techniques as this technique requires a sample core with an L/D ratio of at least 2. Moreover, as the measurements are desired under capillary flow conditions, the steady-state method is found to be more appropriate.

Fig. 1 illustrates the flow patterns in porous media as a function of capillary number and ratio of viscosities of the invading and defending fluids [15]. A schematic of the flow patterns for the three flow regimes is also shown [16]. Transport of liquid water in fuel cells falls in the capillary fingering regime in which the displacement is slow enough so that viscous forces are negligibly small compared to capillary forces. Flow rates for the experiments are carefully selected such that the flow is within the regime of capillary fingering.

2.2. Design of apparatus

2.2.1. Design conditions

Measurement of GDL properties is desired at flow conditions typical of fuel cell operation. At a current density of $1\,A\,cm^{-2}$, the rate of liquid water flow rate is of the order of $0.005\,cm^3\,min^{-1}\,cm^{-2}$, which corresponds to a pore Reynolds of 10^{-6} and a capillary number of 10^{-8} respectively. Similarly, gas velocity in the GDL is of the order of $1\,cm\,s^{-1}$, which is equivalent to an air flow rate of $2.5\,cm^3\,min^{-1}\,cm^{-2}$. The pore Reynolds number for air is about 10^{-4}. The experimental setup is designed with the objective of achieving air and water flow rates as close as possible to those occurring in a fuel cell. The flow-regime zone of experimental conditions is indicated in Fig. 1.

2.2.2. Through-plane test rig

The diameter of the test piece is selected as 0.5 in. (12.7 mm) so that the flow rates are in the range of the metering devices. Flow rates of air and water flow rates are selected as 0–500 sccm and 0–0.5 ccm respectively. In this range, the Reynolds and capillary numbers are only an order of magnitude higher than those in actual fuel cell conditions, but nevertheless they fall in the same flow regime in terms of capillary number and pore Reynolds number (refer Fig. 1).

In order to achieve a mixed, homogenous flow at the inlet to the test specimen, an upstream hydrophilic porous section consisting of a rigid plastic material is used. An L/D ratio of 4 is selected for this upstream section to allow sufficient length for complete mixing. An identical piece is used down-stream of the test specimen in order to minimize any end effects.

Pressure probes are inserted into the porous plastic to measure pressure drop across the test specimen. These probes are fitted with hydrophobic and hydrophilic porous tips in order to separately measure pressure drops for air and water. However, during experiments, liquid and gas pressures could not be satisfactorily isolated in the two-phase region. As an alternative, the pressure drop is measured with respect to the single-phase inlet region both with and without the GDL specimen placed between the porous plastic sections, the difference of which gives the pressure drop across the specimen. With this technique, it is observed that the pressure drop for the liquid and gas phases are equal over the range of flow conditions examined, implying an approximately uniform saturation and hence constant capillary pressure. The pressure drop across the test specimen is thus set equal to its gas-phase pressure drop.

Fig. 2 shows a detailed drawing of the test apparatus. It shows the GDL specimen placed in a donut shaped Teflon gasket and flanked between two identical upstream and downstream cups made of polycarbonate. Cylindrical pieces of porous plastic (from GenPore Inc.), which serve as mixing chambers, are inserted into these cups providing rigid support to the GDL specimen when assembled. Pore size of about 90 μm, an order of magnitude higher than that of GDL materials, is selected for the porous plastic. Sufficient length is provided for the pre-mixing chamber to ensure complete mixing. Stainless steel pressure probes are inserted

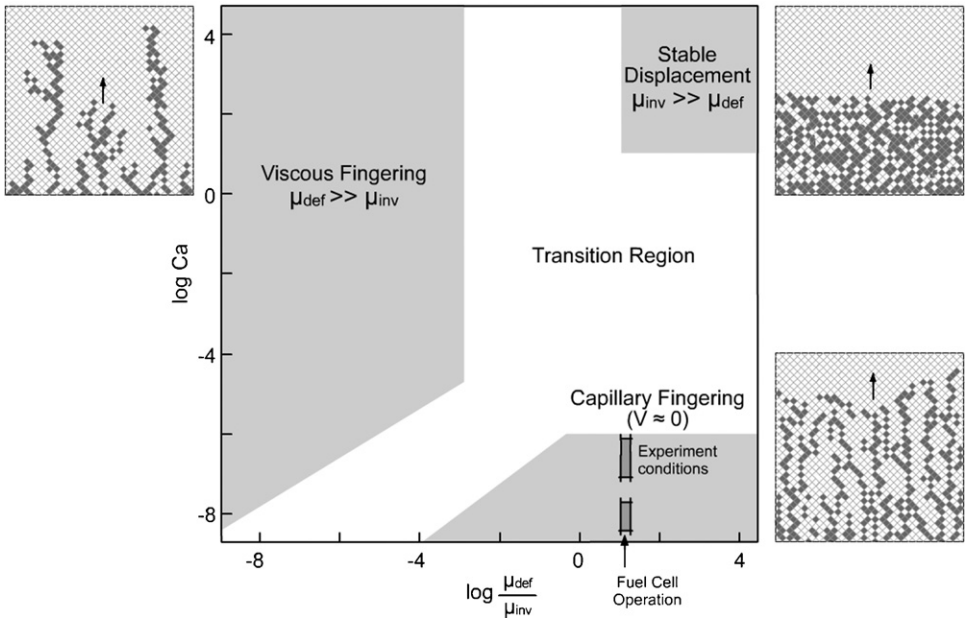

Fig. 1. Flow map for fluid transport through porous media (redrawn after [15,16]).

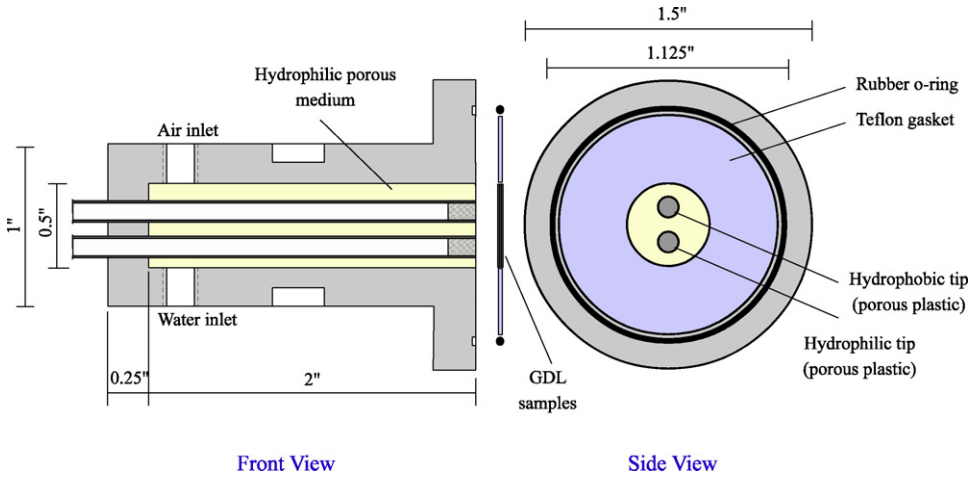

Fig. 2. Design of test rig for through-plane permeability measurements.

through the porous plastic to measure pressure drop across the GDL specimen.

In order to obtain a measurable pressure drop, it is found necessary to use a stack of a few layers of GDL material. The number of layers used and the resulting compression are given in Table 1. A rubber o-ring around the periphery of the gasket serves to provide an air-tight assembly. Vee-blocks are used for aligning the two halves of the test rig. The assembly is held together by three vise grips around the periphery that allow for quick removal of the sample for measuring saturation. The whole assembly is tested for leaks at a pressure of 25 psig. A picture of the fabricated through-plane test rig is shown in Fig. 4(a).

2.2.3. *In-plane test rig*

Fig. 3 shows the design of the test rig for in-plane measurements. In this case, the specimens are rectangular in shape with 0.25 in. (6.4 mm) width and 1 in. (25.4 mm) length placed in Teflon gasket with a rubber o-ring gasket around its periphery. Two layers of GDL are used in order to achieve proper compression and a leak-tight assembly. The specimen is flanked between two rectangular polycarbonate blocks as shown. Air and water enter from one end on opposite faces of the specimen, pass through the GDL in the in-plane direction and exit out from the other end as a two-phase mixture. The range of air and water flow rate are selected as 0–50 sccm and 0–0.015 ccm respectively. As the flow length is

Table 1
Details of test specimen for through-plane measurements.

Material	Thickness (μm)	Gasket thickness (μm)	Number of layers	Compression (%)
Toray-060	203	762	4	6
Toray-090	280	762	3	9
Toray-120	356	1651	5	7
E-Tek cloth	280	1651	7	16

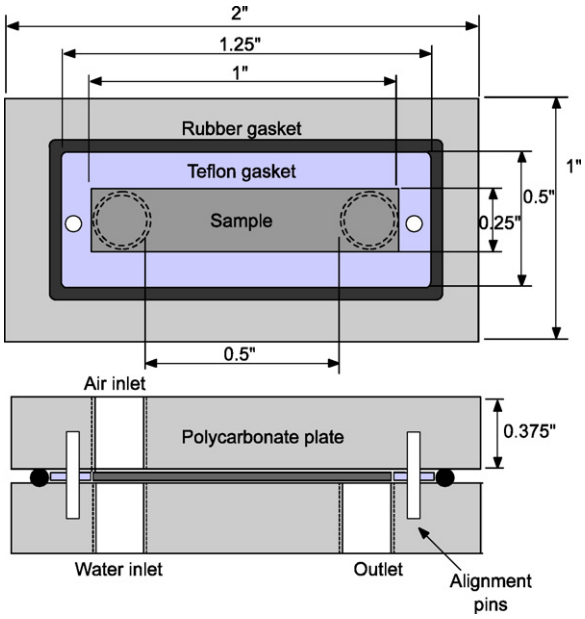

Fig. 3. Design of test rig for in-plane permeability measurements.

about two orders of magnitude longer than the hydraulic diameter, pre-mixing sections are not required. Alignment pins are used to position the gasket and specimens within the assembly. Vise grips are used achieve a leak-tight assembly and to allow for quick removal of GDL samples. A picture of the fabricated test rig is shown in Fig. 4(b).

2.3. Absolute permeability

Absolute permeability is measured by applying Darcy's law for a single-phase fluid (dry air) under steady-state conditions. At each flow rate, pressure gradient is measured and plotted against superficial velocity. Flow rates of 0–500 sccm for through-plane measurements and 0–50 sccm for in-plane measurements are used. At sufficiently low velocities, inertial forces (or Forchheimer effects) are negligible and a linear relationship would exist between pressure gradient and superficial velocity. Absolute permeability is calculated using the following equation in which the denominator represents the slope of the straight line obtained from the plot.

$$k = \frac{\mu_a}{(\Delta p_a/\Delta x)/u_a} \tag{3}$$

2.4. Porosity

Porosity refers to the fraction of fluid-accessible void space present in a porous material. Its value is needed for calculating saturation. Porosity of GDL materials is known to vary slightly from batch to batch and is not always available from the manufacturer. It is therefore decided to measure it in the laboratory for the specimens under consideration.

Table 2
Thickness of GDL specimens and their calculated porosities and uncertainties.

Material	Dry mass (mg)	IPA-saturated mass (mg)	Porosity ε_0
Toray-060	53.0	130.4	0.76 ± 0.038
Toray-090	79.2	180.3	0.72 ± 0.026
Toray-120	105.8	234.8	0.72 ± 0.021
E-Tek cloth	68.2	181.0	0.80 ± 0.029

Several methods are available for measuring porosity [17]. In this work, the method of liquid saturation is selected due to its simplicity and reasonably good accuracy [18]. The method involves saturating the specimen with a suitable wetting fluid and measuring the gain in mass. Porosity of the bare specimen (uncompressed) is then calculated from the equation

$$\varepsilon_0 = \frac{V_{\text{pore}}}{V_{\text{total}}} = \frac{\Delta m/\rho_l}{At_0} \tag{4}$$

Circular pieces of 1.125 in. diameter are used for these measurements. High purity isopropyl alcohol (IPA) is selected as the wetting fluid as it spontaneously wets the GDL materials and can therefore be assumed to invade all accessible pores. Density of IPA at room temperature is taken as 786 kg m^{-3} [19]. Table 2 lists the materials, measured mass under dry and saturated conditions and calculated porosity and corresponding uncertainty. Details of uncertainty analysis are given in Section 2.8.

Porosity of a material decreases when compressed. Under moderate compression, it may be assumed that the solid volume remains unchanged and only the pore space gets reduced. Neglecting any changes in lateral dimensions, porosity under compression can be calculated from the equation [20]:

$$\varepsilon_c = \frac{\varepsilon_0 - c}{1 - c} \tag{5}$$

where c is the linear compression given by

$$c = 1 - \frac{t_c}{t_0} \tag{6}$$

2.5. Saturation

Saturation is defined as the fraction of total pore space occupied by liquid water. Both in situ and ex situ techniques have been reported in literature for measuring saturation. In situ methods have the advantage of high accuracy but require complex facilities such as x-ray tomography, gamma ray detectors and neutron radiography [21–23]. Ex situ methods, however, have moderate accuracy and are relatively simple but they require a suitably designed appa-

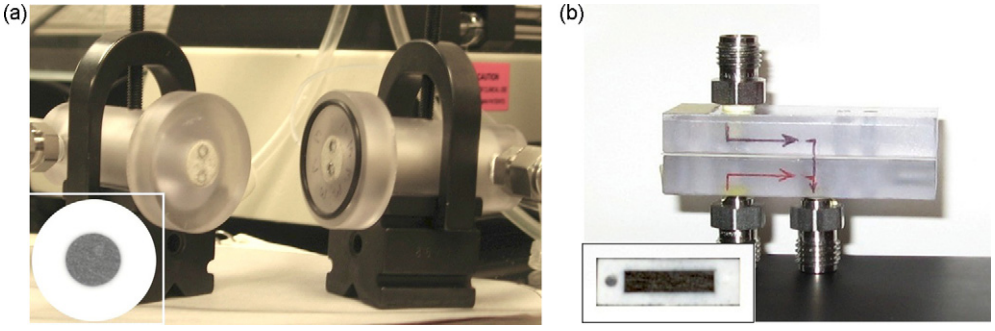

Fig. 4. Pictures of test rig for (a) through-plane and (b) in-plane measurements. Inset shows the GDL samples placed in Teflon gaskets.

ratus depending on whether the volumetric or the gravimetric method of measurement is used [7,8,24].

In this work, the ex situ gravimetric method of measurement is selected. This method involves swift removal of the sample from the test rig to measure mass gained with reference to its dry state. Average saturation is then calculated from the equation:

$$s = \frac{\Delta m/\rho_w}{\varepsilon_c A t_c} \tag{7}$$

2.6. Relative permeability

As mentioned earlier, steady-state methods are found to be more suitable for measuring relative permeability at the flow conditions desired. Steady-state techniques rely on direct application of Darcy's law. The two fluids are pumped through the sample at known flow rates until steady state is achieved indicated by a constant pressure drop with time. With other parameters known, Eq. (1) is used to calculate relative permeability $k_{r,i}$. Flow rates are then varied in a systematic manner in order to achieve increasing saturations. Before each test, the GDL specimens are air-dried in order to remove any pre-existing water from the pores. The initial state of zero saturation is verified by comparing the weight of the test pieces with that of an oven-dried sample.

2.7. Instrumentation and test conditions

Flow rate of air is controlled by a digital mass flow controller (Omega FMA 2619A) and that of water is controlled by a syringe pump (Harvard Apparatus Model 22). Mass of the GDL specimens is measured with a digital weighing scale (Denver Instruments XE-50 ±0.1 mg). Pressure drop is measured using a differential pressure gauge (Dwyer Instruments Magnehelic® gauge, ranges of 1, 5 and 10 in. water). In through-plane experiments, air and water flow rates are varied from 500 to 0 sccm and 0 to 0.5 ccm respectively. In the in-plane experiments, they are varied from 50 to 0 sccm and 0 to 0.015 ccm respectively. Saturated air is used in two-phase relative permeability experiments. All measurements are performed at room temperature.

2.8. Uncertainty analysis

The uncertainty in a multi-variable function $Y = Y(X_1, X_2, \ldots X_N)$ due to uncertainties in variables $X_1, X_2, \ldots X_N$ is given by the root sum square product of the individual uncertainties computed to first-order accuracy as [25]:

$$U_Y = \left[\sum_{i=1}^{N}\left(\frac{\partial Y}{\partial X_i}U_{X_i}\right)^2\right]^{1/2} \tag{8}$$

The above equation forms the basis for uncertainty analysis. Physically, the partial derivative represents the sensitivity of Y to the variable X_i and therefore it is also referred to as the sensitivity coefficient. Eq. (8) applies as long as each measurement of Y is independent and repeated measurements exhibit Gaussian distribution. Uncertainty in the values of the independent variable (U_{X_i}) represents the band within which the true value of X_i is expected to lie with a certain level of confidence. Typically, a confidence level of 95% is used at which U_X is equal to 2σ, where σ is the standard deviation [26].

Depending on the complexity of the function $Y(X_i)$ and the number of variables involved, uncertainty may be calculated either analytically or computationally [25]. In the computational scheme, the partial derivative in Eq. (8) is replaced by a ratio of discrete changes to give

$$U_Y = \left[\sum_{i=1}^{N}\left(\frac{\Delta Y_i}{\Delta X_i}U_{X_i}\right)^2\right]^{1/2} \tag{9}$$

in which ΔX_i and ΔY_i are given by

$$\Delta X_i = 2U_{X_i} \tag{10}$$

$$\Delta Y_i = Y_{X_i^+} - Y_{X_i^-} \tag{11}$$

$$Y_{X_i^+} = Y(X_1, X_2, \ldots, X_i + U_{X_i}, \ldots, X_N) \tag{12}$$

$$Y_{X_i^-} = Y(X_1, X_2, \ldots, X_i - U_{X_i}, \ldots, X_N) \tag{13}$$

Table 3 gives the uncertainties in independent variables considered in the present study. The value of uncertainties in independent variables are obtained either from manufacturer's specifications for the instrument or from measurements taken in laboratory. Calculation of uncertainties is performed using the software Engineering Equation Solver (EES) [27].

3. Results and discussion

3.1. Absolute permeability

Fig. 5 shows plot of pressure gradient versus superficial velocity for the through- and in-plane permeability experiments, with air as the working fluid. Calculated values of absolute permeability in darcy are also shown in the figure. Linear relationship between pressure gradient and superficial velocity clearly demonstrates absence of inertia effects in both cases. Error bars correspond to the uncertainty in the calculated value due to uncertainties in other independent variables.

As per manufacturer's specifications, the three carbon paper GDLs are structurally similar and differ only in their thicknesses. Hence, their pore structures and resulting permeabilities are expected to be about the same. The difference observed in their measured values can therefore be attributed to the difference in their compressions. From the data shown in Fig. 5(a) for Toray-090 and Toray-120, it is seen that the permeability of the material is strongly dependent on its compression. Toray-060 however, shows a higher permeability than the rest which is possibly due to the higher porosity of this material (refer Table 2).

In-plane permeabilities are shown in Fig. 5(b). Some degree of anisotropy is observed between through- and in-plane permeabilities. Consider, for example, Toray-090 which has identical compression in both through and in-plane experiments. Its in-plane value is found to be higher by about 18%. In comparison, Gostick et al. report in-plane values to be higher by 30% [20].

Permeability of carbon cloth is found to be higher in the through-plane than in the in-plane direction by a factor of about 1.75. It is due to the weave pattern of the cloth which results in tighter spaces in along-fiber direction unlike carbon paper in which the fibers are distributed fairly evenly.

Table 4 gives a summary of measured absolute permeabilities and a comparison with the values reported in literature. Compression at which the values have been calculated is also given. It is seen that values obtained in the present work are slightly higher but generally in the range reported by other researchers under similar compression conditions, thus providing confidence in the apparatus and the experimental technique.

Measurement of absolute permeability in the in-plane direction is also undertaken using fluids other than air such as IPA and water. GDL materials are inherently hydrophilic to IPA which enables the fluid to spontaneously invade the entire pore-space. With water however, the materials are known to exhibit mixed wettability [9].

Table 3
List of independent variables and their uncertainties.

Parameter	Value/range	Uncertainty	Source
1. Porosity measurement			
Specimen diameter, D	28.575 mm	±0.100 mm	Measured
Thickness, t_0	(Table 1)	±0.010 mm	Measured
Mass, Δm	–	±0.1 mg	Instrument spec.
2. Through-plane experiments:			
Specimen diameter, D	12.7 mm	±0.100 mm	Measured
Gasket thickness, Δx	762, 1651 μm	±0.020 mm	Measured
Pressure drop, Δp	1 in. water FSR	±2% FSR	Instrument spec.
	5 in. water FSR	± 2% FSR	Instrument spec.
Air flow rate, Q_a	0–500 sccm	± (0.8% + 0.2% FSR)	Instrument spec.
Water flow rate, Q_w	0–0.5 ccm	±2%	Assumed
Mass, Δm	–	±0.1 mg	Instrument spec.
3. In-plane experiments:			
Gasket thickness, t_c	508, 584 μm	±0.020 mm	Measured
Specimen width, w	12.7 mm	±0.010 mm	Measured
Length (for saturation), L	25.4 mm	±0.100 mm	Measured
Length (for pr. drop), Δx	12.7 mm	±0.100 mm	Measured
Pressure drop, Δp	10 in. water FSR	± 2% FSR	Instrument spec.
Air flow rate, Q_a	0–50 sccm	± (0.8% + 0.2% FSR)	Instrument spec.
Water flow rate, Q_w	0–0.15 ccm	±2%	Assumed
Mass, Δm	–	±0.1 mg	Instrument spec.

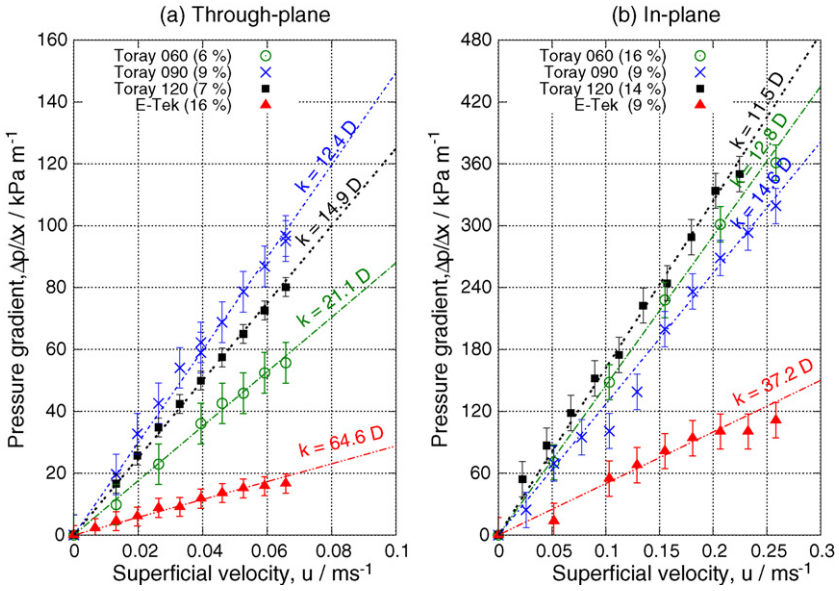

Fig. 5. Measurement of absolute permeability. Compression of each sample is shown in the legend.

Table 4
Comparison of through- and in-plane permeabilities. [a]

Material	Through-plane		In-plane	
	Literature	This work	Literature	This work
Toray-060	$5–10_{0\%}$ [30]	$21.1^{\pm 2.62}_{6\%}$	$5–10_{75\%}$ [30]	$12.8^{\pm 1.68}_{16\%}$
Toray-090	$9_{10\%}$ [20] $4.4_{5\%}$ [8]	$12.4^{\pm 0.88}_{9\%}$	$20_{0\%}$ [20]	$14.6^{\pm 2}_{9\%}$
Toray-120	$8.7_{0\%}$ [18]	$14.9^{\pm 0.61}_{7\%}$	n/a	$11.5^{\pm 1.53}_{14\%}$
E-Tek	$55_{0\%}$ [30] $69.4_{0\%}$ [20] $47_{0\%}$ [18] $13_{60\%}$ [31]	$64.6^{\pm 13.4}_{16\%}$	 $30_{10\%}$ [20] $17.4_{50\%}$ [31]	$37.2^{\pm 11.4}_{9\%}$

[a] All values are in darcy. The level of compression is given as a subscript. The uncertainty in calculated value is given as a superscript alongside experimental results.

If the flow rate of water is maintained high enough, the liquid pressure is also high and hence it is possible for water to invade all pores achieving a saturation close to 100%. Measurements are conducted for Toray-090 carbon paper in the in-plane direction. Fig. 6 shows a plot of pressure gradient versus the parameter $u\mu$ with IPA and water, together with the data using air. The data points are found to lie close to the same straight line. The absolute permeability (reciprocal of slope) is found to be 13.2 darcy, which is about 10% lower than its value using dry air as the working fluid. The difference is apparently due to presence of a small fraction of un-invaded pores.

3.2. Saturation—capillary number relationship

Fig. 7 shows the measured liquid water saturation plotted against capillary number. Capillary number in experimental measurements is low enough for surface tension effects to be significant and is about an order of magnitude higher than that occurring in actual fuel cell operation. From the experimental results, it is

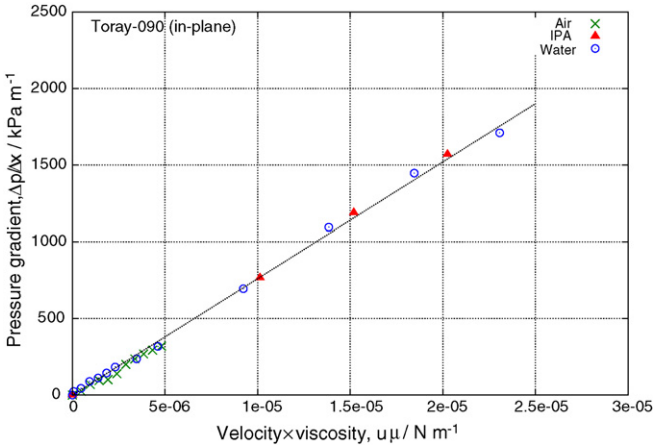

Fig. 6. Measurement of absolute permeability of Toray-090 carbon paper using air, water and IPA.

found that saturation varies linearly with capillary number. This is expected because a higher capillary number implies higher liquid water flow rate and hence proportionately more pores filled with liquid water. For Toray carbon paper, saturations are slightly higher in the in-plane direction than in the through-plane as evident from the slope. The three carbon paper materials show identical trends due to similarity in their fibrous micro-porous structures.

Carbon cloth, however, shows higher saturations in the through-plane than in the in-plane. This is due to its higher through-plane absolute permeability and hence a higher median pore size in that direction.

3.3. Water relative permeability

Fig. 8 shows the relative permeability of water plotted against saturation in the through- and in-plane directions for the GDL materials under consideration. In this case too, the three carbon paper materials demonstrate similar trend due to similarity in their pore structures. A best-fit line of the form $k_{r,w}(s) = s^n$ is then determined. For the range of flow conditions considered in this study, a value of 5.5 is obtained for n. Water relative permeability is found to be below the generally assumed s^3 function by a factor of about 25 in the observed range. Measured values for carbon paper are comparable to those reported by Sole et al. for Toray-090 [8]. Through-plane permeability for carbon cloth is found to lie along the $0.01s^3$ line for $0 \le s \le 0.8$. No prior measurements are available in the literature for E-Tek carbon cloth for a one-on-one comparison.

In-plane relative permeability measurements given in Fig. 8(b) show higher values compared to their through-plane counterpart. Observed trend fits the function $k_{r,w}(s) = s^4$ for $0 \le s \le 0.5$, confirming the theoretical speculation first proposed by Luo et al. [28] and Ju et al. [29]. Data for Toray-060 carbon paper in the in-plane direction could not be obtained with sufficient accuracy and repeatability and is hence omitted.

From experimental data, it is seen that at a given saturation, in-plane relative permeability is higher than its through-plane value. Physically, this implies that the pore-network is more conducive to the movement of water in the in-plane than in the through-plane. Further studies using topologically equivalent pore network models will help shed more light on this anisotropic phenomenon.

3.4. Air relative permeability

Fig. 9 shows relative permeability of air ($k_{r,a}$) plotted against saturation for the through- and in-plane directions for the two GDL materials. Experimental data reported by Koido et al. [7] are also shown for comparison in Fig. 9(a). The difference between the two sets of data could be due to the fact that the present work is conducted at flow conditions in the capillary fingering regime. Details of flow rate conditions in Koido's work are not reported. In Sole's work too [8], focus is on measurement of water relative permeability and hence air relative permeability results are not presented.

In this study, the calculated values of $k_{r,a}$ in the through-plane are found to be unrealistically low. This appears to be an experimental artifact and possible causes are discussed in more detail in the next section.

Data in the in-plane direction is more consistent and reliable. For carbon paper, $k_{r,a}$ is found to follow the $(1 - s^2)^4$ trend, whereas for carbon cloth, it is found to lie along the $(1 - s)^3$ line.

Data points with error bars reflecting uncertainty in measurement of saturation and calculated relative permeability of water and air are shown in Fig. 10(i) and (ii) respectively. Higher uncer-

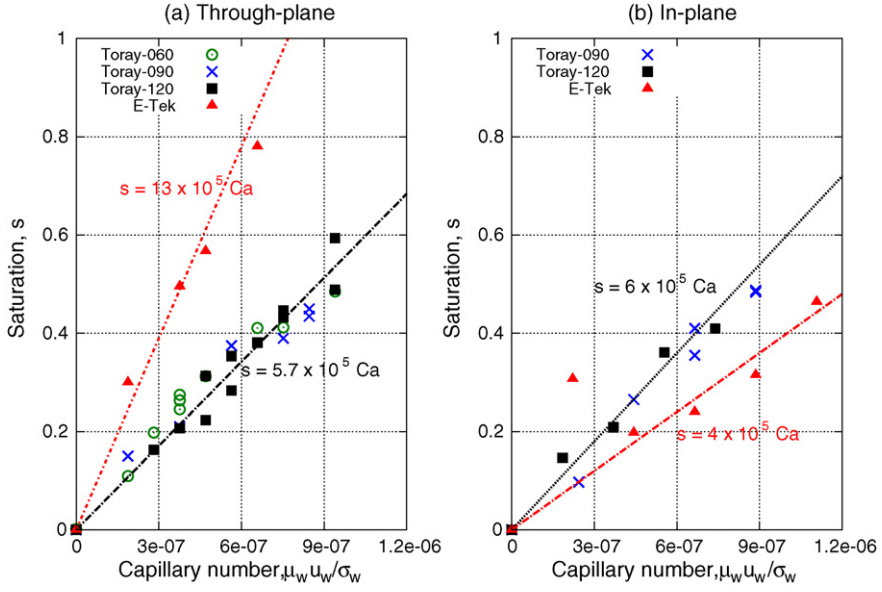

Fig. 7. Measured liquid water saturation as a function of capillary number.

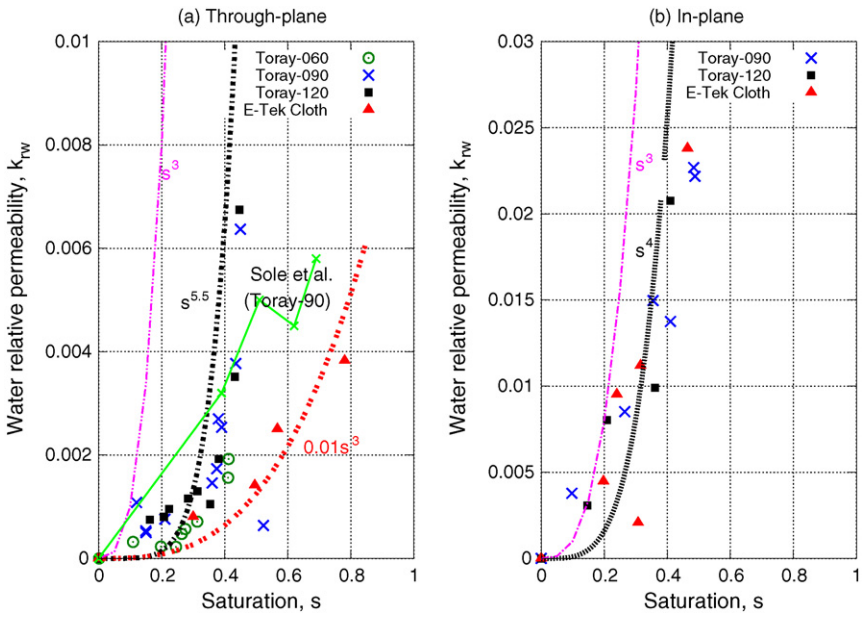

Fig. 8. Water relative permeability in through- and in-plane directions for carbon paper and carbon cloth GDLs.

tainties with increasing saturations are due to the fact that at higher saturations, air flow rate is decreased and water flow rate is increased, which together result in smaller pressure drop. At low pressure drop, the uncertainty in its value is magnified which then reflects as a higher uncertainty in calculated relative permeability.

3.5. *Effect of stacking and other non-uniformities on through-plane measurements*

In through-plane experiments, a few layers of gas diffusion material are stacked together in order to achieve a measurable pressure drop. With stacking, there is a possibility of liquid water accumulating in the thin interfacial gap between various layers. Presence of this thin film of water will potentially affect the measured air and water relative permeability. It is therefore desired to see what effect, if any, stacking has on the measured relative permeabilities of air and water.

In order to explore this, results from a 3-layer stack of Toray-090 carbon paper are compared against those from a 9-layer stack of same material. The number of interfaces in the two stacks are 2 and 8 respectively.

Fig. 11 shows the experimental measurement of air and water relative permeability for the two stacks. The data is found to be generally within the range of experimental scatter. On the basis of these results, it may be concluded that varying the number of layers does not have any significant effect on the measured parameters. Scatter observed in the data is attributed to the general randomness of two-phase flow in porous structures.

Another factor that may play a role is the non-uniformity of saturation in the test specimen. One of the assumptions on which

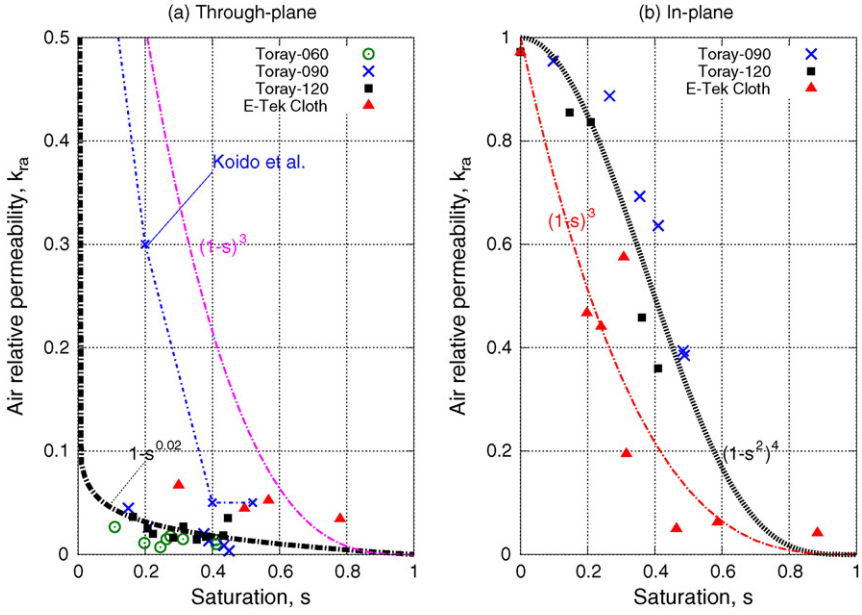

Fig. 9. Air relative permeability in through- and in-plane directions for carbon paper and carbon cloth GDLs.

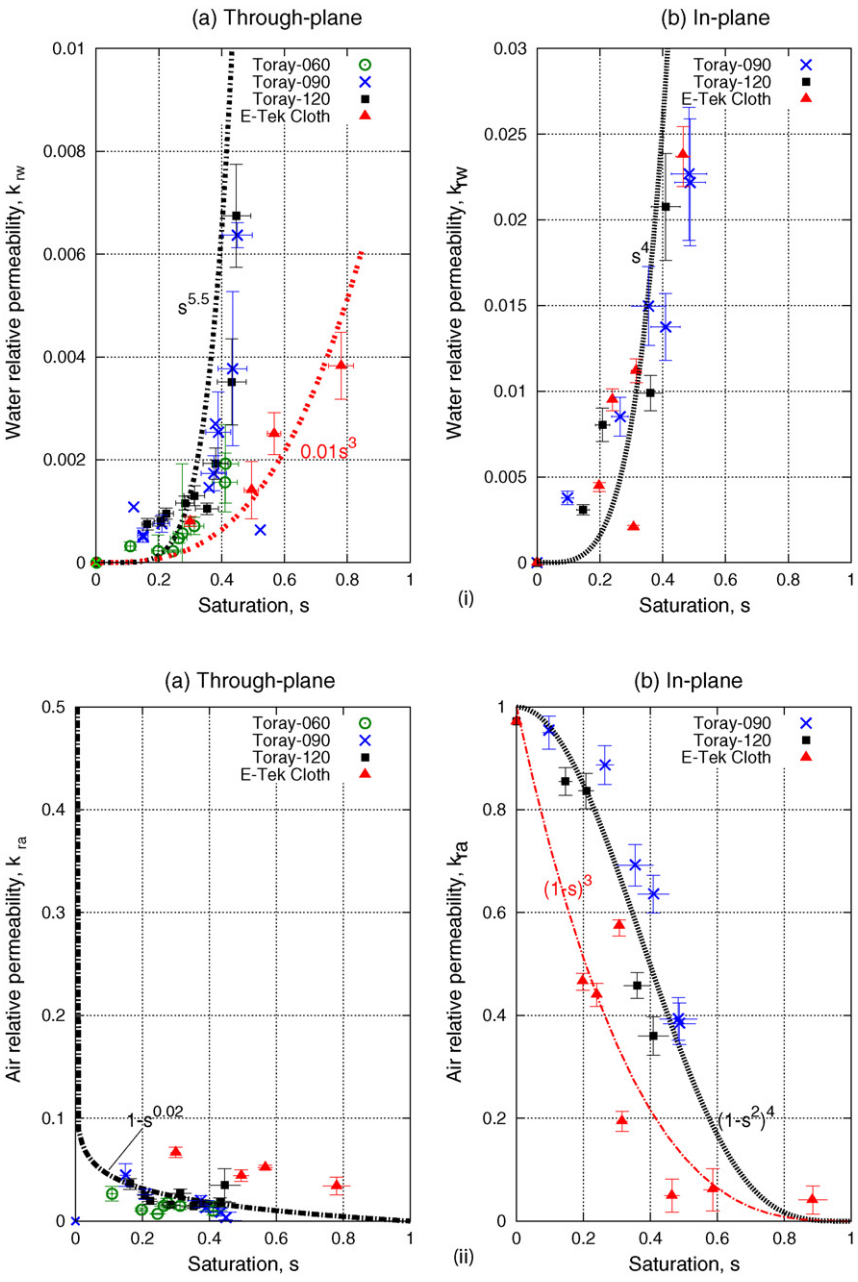

Fig. 10. Water and air relative permeability in through- and in-plane directions with error bars.

these experiments are based is that the gradient in saturation is small so that it may be represented by a volume-averaged value. However, some variation in saturation is expected in experiments due to factors such as presence of non-uniformities in the material and effect of interfaces between layers. The extent of variation in saturation along the different layers in the stack is examined here.

Fig. 12 shows the variation in saturation along each of the nine individual layers in the Toray-090 stack for two through-plane cases that represent extremeties of saturation conditions. It is observed that the layers at either end of the stack show higher saturation compared to those in the interior of the stack. The trend is similar for the two cases considered. This is apparently due to accumulation of water in the non-uniformities at the interface between the machined porous plastic inserts and the GDL material. The net effect is that the apparent saturation is higher which shifts the $k_{r,w}$ and $k_{r,a}$ curves to the right and left respectively.

From Fig. 12, it is seen that if the contribution of the end layers is factored out, a better approximation of uniform saturation may be achieved. Relative permeability based on average saturation is related to relative permeability of each layer through the equation:

$$k_r(s_{\text{avg}}) = n\delta \left(\int_{x=0}^{n\delta} \frac{\mathrm{d}x}{k_r(s_x)} \right)^{-1} \tag{14}$$

where δ and n represent the thickness of each layer and the number of layers respectively. Table 5 shows a comparison of estimated saturation and relative permeability values for the stack, with and without the end layers being considered. Relative permeability is assumed to be a cubic function of saturation in these calculations. Of all the parameters, air relative permeability shows the maximum error of the order of 200%, indicating that it is highly sensitive to variations in saturation and pressure drop.

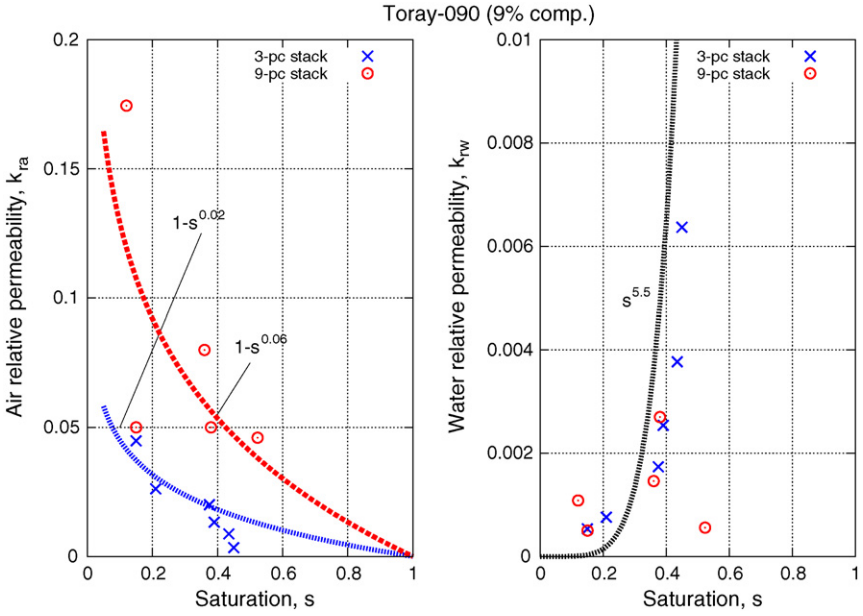

Fig. 11. Relative permeabilities in through-plane direction using 3- and 9-layered stacks of Toray-090 at 9% compression.

Table 5
Effect of non-uniformities in saturation on calculated parameters.

Parameter	Case I (Q_a/Q_w = 400/0.1 ccm)			Case II (Q_a/Q_w = 100/0.4 ccm)		
	Layers 1–9	Layers 2–8	% Error	Layers 1–9	Layers 2–8	% Error
s_{avg}	0.097	0.064	+34	0.523	0.468	+11
$k_{r,a}$	0.710	0.820	−16	0.046	0.144	−213
$k_{r,w}$	0.000251	0.000196	+22	0.110	0.095	+14

The accumulation of water in the end layers could potentially be the reason for the low relative permeability of air that is observed in through-plane experiments. To effectively eliminate these non-uniformities, pressure probes need to be inserted through the end layers and pressure drop recorded in the interior of the specimens. An in situ method of measuring saturation will have to be adopted. This is a design improvement that may be incorporated in future studies. Results obtained for in-plane experiments are, however, unaffected by this phenomenon as the length of the specimen in this case is about 50 times higher than its hydraulic diameter.

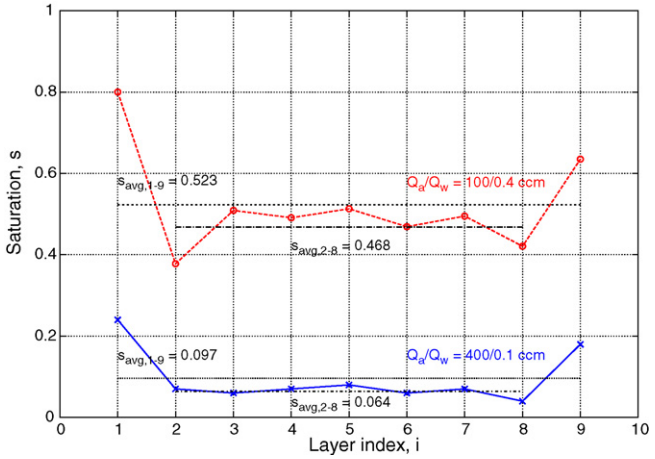

Fig. 12. Variation of saturation across the layers in the stack.

4. Conclusions

In this study, experimental measurement of absolute permeability and air–water relative permeability functions for typical fuel cell GDL materials such as Toray carbon paper (TGP-H-060, -090, -120) and E-Tek carbon cloth have been presented. Measurements in both through- and in-plane directions have been performed at flow conditions corresponding to the capillary fingering flow regime. Following are the main conclusions drawn from this study:

1. For carbon paper materials, absolute permeabilities in the in-plane directions are found to be higher than their through-plane values by about 18%, whereas for carbon cloth, through-plane permeability is found to be higher by about 75% than its in-plane value.
2. Liquid water saturation is found to be a linear function of capillary number. At a given capillary number, carbon papers show similar saturation in through- and in-plane directions whereas carbon cloth shows higher saturation in the through-plane than in the in-plane.
3. Through-plane k_r measurements exhibit large uncertainties. Accumulation of water in the end layers is identified as a major cause for uncertainty in calculations. Possible measures to minimize these errors have been suggested.
4. In-plane data are more reliable with much less uncertainty. Recommended k_r expressions for in-plane direction are

$$k_{r,w} = s^4 \quad \text{(for carbon paper and cloth)}$$

$$k_{r,a} = (1 - s^2)^4 \quad \text{(for carbon paper)}$$

$$= (1 - s)^3 \quad \text{(for carbon cloth)}$$

5. A careful uncertainty analysis has been performed in this study, which will guide future efforts in k_r measurement. Experimental data of k_r are presented with error bars for the first time in the literature.

Acknowledgements

Funding for this work from ECEC industrial sponsor is gratefully acknowledged. I.S.H. also acknowledges King Abdullah University of Science and Technology (KAUST), Saudi Arabia for a fellowship award.

References

[1] J. Larminie, A. Dicks, Fuel Cell Systems Explained, 2nd ed., John Wiley & Sons Ltd., New York, 2003.
[2] C.Y. Wang, Chem. Rev. 104 (10) (2004) 4727–4766.
[3] Z.H. Wang, C.Y. Wang, K.S. Chen, J. Power Sources 94 (1) (2001) 40–50.
[4] H. Darcy, The Public Fountains of the City of Dijon, Kendall/Hunt Pub. Co., Dubuque, Iowa, 1856.
[5] J.T. Gostick, M.A. Ioannidis, M.W. Fowler, M.D. Pritzker, in: U. Pasaogullari, C.Y. Wang (Eds.), Modeling and Diagnostics of Polymer Electrolyte Fuel Cells, Springer Pub. Co., New York, 2010.
[6] T.V. Nguyen, L. Guangyu, O. Heebong, H. Dan, J. David, A. Muhammad, ECS Trans. 3 (1) (2006) 415–423.
[7] T. Koido, T. Furusawa, K. Moriyama, K. Takato, ECS Trans. 3 (1) (2006) 425–434.
[8] J.D. Sole, Investigation of water transport parameters and processes in the gas diffusion layer of PEM fuel cells, PhD dissertation, Virginia Polytechnic Institute and State University, 2008.
[9] P. Sinha, C. Wang, Electrochim. Acta 52 (28) (2007) 7936–7945.
[10] J. Gostick, M. Ioannidis, M. Fowler, M. Pritzker, J. Power Sources 173 (1) (2007) 277–290.
[11] B. Markicevic, A. Bazylak, N. Djilali, J. Power Sources 171 (2) (2007) 706–717.
[12] M. Honarpour, L. Koederitz, A. Harvey, Relative Permeability of Petroleum Reservoirs, CRC Press, 1986.
[13] S.E. Buckley, M.C. Leverett, Trans. AIME 146 (1942) 107–116.
[14] H.J. Welge, J. Petrol. Technol. 4 (4) (1952) 91–98.
[15] E.T.R. Lenormand, C. Zarcone, J. Fluid Mech. 189 (1988) 165–187.
[16] E. Aker, K. Jørgen Måløy, A. Hansen, G. Batrouni, Transport Porous Med. 32 (2) (1998) 163–186.
[17] J. Bear, Dynamics of Fluids in Porous Media, Dover Publications, 1988.
[18] M. Williams, E. Begg, L. Bonville, H. Kunz, J. Fenton, J. Electrochem. Soc. 151 (2004) A1173–A1180.
[19] C. Yaws, Chemical Properties Handbook, McGraw-Hill, New York, 1999.
[20] J.T. Gostick, M.W. Fowler, M.D. Pritzker, M.A. Ioannidis, L.M. Behra, J. Power Sources 162 (1) (2006) 228–238.
[21] H.O. Schiegg, J.F. McBride, D.N. Graham, Laboratory Setup and Results of Experiments on Two-dimensional Multiphase Flow in Porous Media, Pacific Northwest Laboratory, 1990.
[22] J. Schembre, A. Kovscek, J. Petrol. Sci. Eng. 39 (1–2) (2003) 159–174.
[23] P. Sinha, P. Halleck, C. Wang, Electrochem. Solid State Lett. 9 (7) (2006) A344–A348.
[24] A. Demond, P. Roberts, Water Resour. Res. 29 (4) (1993) 1081–1090.
[25] R.J. Moffat, Exper. Therm. Fluid Sci. 1 (1) (1988) 3–17, doi:10.1016/0894–1777(88)90043-X.
[26] J. Kim, T. Simon, R. Viskanta, J. Heat Transf. 115 (1993) 5–6.
[27] S. Klein, F. Alvarado, Engineering Equation Solver, F-Chart Software, Middleton, Wisconsin, 2009.
[28] H. Ju, G. Luo, C. Wang, J. Electrochem. Soc. 154 (2007) B218–B228.
[29] G. Luo, H. Ju, C. Wang, J. Electrochem. Soc. 154 (2007) B316–B321.
[30] M. Mathias, J. Roth, J. Fleming, W. Lehnert, in: W. Vielstich, H.A. Gasteiger, A. Lamm (Eds.), Handbook of Fuel Cells Fundamentals, Technology and Applications, vol. 3, John Wiley & Sons Ltd., 2003.
[31] V. Gurau, M.J. Bluemle, E.S. DeCastro, Y.-M. Tsou, T.A. Zawodzinski, J.A. Mann, J. Power Sources 165 (2) (2007) 793–802.